Stochastic modelling for virtual engineering of controlled atmosphere storage of fruit

Q.Tri Ho[1], Seppe Rogge[1], Pieter Verboven[1], Bert E. Verlinden[2], Bart M. Nicolaï[1,2]

[1]BIOSYST-MeBioS, KU Leuven, Willem de Croylaan 42, B-3001 Leuven, Belgium.

[2]Flanders Centre of Postharvest Technology, Willem de Croylaan 42, B-3001 Leuven, Belgium.

Corresponding author: Quang Tri Ho

E-mail: quangtri.ho@biw.kuleuven.be

Tel: 32-16-32 05 88 fax: 32-16-32 29 55

Abstract

Long term storage of pear fruit requires low temperature and conventionally uses controlled atmosphere (CA) conditions to reduce respiration and consequent quality loss. Sub-optimal storage conditions may lead to physiological disorders and loss of product. Stochastic variability of the properties of fruit introduces uncertainty in storage design and operations and could result in severe quality loss. Taking such variability into account in simulation models for virtual engineering will allow to assess the uncertainty of the process and determine confidence limits for the operation. Gas exchange in pear fruit during controlled atmosphere storage was studied using a continuum diffusion-respiration model, taking into account stochastic variation of the 3D morphology, the diffusivity of oxygen and carbon dioxide and the maximal respiration rate. Different geometries were generated using a statistical shape generation algorithm for 3D morphology, that was automatically incorporated into the gas exchange model. Similarly, tissue diffusivity was computed using a 3D tissue microstructure database. Simulation results showed that internal O_2 and CO_2 gas profiles in fruit were highly affected by variation of diffusivities,

maximal respiration rate and the 3D morphology of fruit. The model was further used to evaluate incidence to fermentation at different reduced O_2 levels of storage condition. The risk of fermentation inside the fruit predicted by the gas exchange model rapidly increased in response to decreasing external O_2 levels. The virtual simulation tool confirms that picking time and fruit size are important criteria for proper control of CA storage. While applied here to pear fruit, it can easily be extended to other commodities.

Highlights

- A virtual engineering tool for controlled atmosphere storage of fruit is presented
- A 3D shape generator of fruit is combined with a diffusion-reaction model
- The model predicts critical oxygen levels for development of disorders
- Random model parameters were incorporated
- Fruit size and maturity affect gas concentrations within the fruit the most

Key words

3D modeling, X-ray micro-CT, mass transfer, respiration, finite element method, biological variability, microstructure.

1. Introduction

Pome fruit are an important fresh food product consumed worldwide. After harvest, fruit are often stored under controlled atmosphere (CA) conditions with reduced O_2 and increased CO_2 levels in combination with a low temperature to extend their commercial storage life. In such conditions, gas exchange inside the fruit affects the respiration process. Bad engineering and control of the storage rooms may result in sub-optimal storage conditions that may lead to physiological disorders and loss of product. In 'Conference' pears (*Pyrus communis* L.), the physiological disorder is characterised by softening and browning of tissue near the core and is associated with the development of cavities (Franck et al., 2007; Veltman et al., 2003a, 1999) that cause economic losses (Lammertyn et al., 2000; Veltman et al., 2003a; Zerbini and Rizzolo, 2002). The main hypothesis for explaining the occurrence of browning is that hypoxia inside the fruit might occur, followed by a switch from respiration to fermentation. The low energy yield of the latter is insufficient for repairing membrane damage, and cell death may result (Herremans et al., 2013a, 2013b; Ho et al., 2011; Lammertyn et al., 2000; Pedreschi et al., 2009; Peppelenbos and Oosterhaven, 1998; Saquet et al., 2003; Streif et al., 2003; Veltman et al., 2003b; Zhou et al., 2014). The development of disorders during postharvest ripening and storage of fruit also depends on a range of preharvest factors such as climate conditions. Other factors that have been considered to be influencing the development of the disorder are the size/weight of the fruit and the picking date (Ho et al., 2010a; Lammertyn et al., 2000; Li et al., 2011). Over-mature (late picked) and large fruit have been shown to be more susceptible to core breakdown during storage (Franck et al., 2007; Lammertyn et al., 2000; Verlinden et al., 2002).

Computer aided engineering through mathematical modelling of the process has been used as a tool for quantification of the fruit quality during storage (Bosch et al., 2013; Fukuda et al., 2014;

Ho et al., 2013; Pinheiro et al., 2013). As there are no noninvasive measurement techniques available for monitoring respiratory gas concentrations in fruit during CA storage, gas transport models have been used to evaluate gas transport and respiratory gaseous exchange of fruit. We have previously developed models operating at different spatial scales, from the macroscale (Ho et al., 2011, 2008; Lammertyn et al., 2003; Mannapperuma et al., 1991; Verboven et al., 2013) to the microscale level (Ho et al., 2011, 2009; Verboven et al., 2013, 2012) in a multiscale framework and validated them successfully for different apple and pear fruit cultivars (Ho et al., 2010b, 2008). Such modelling has shown that the local gas concentrations and the respiration rate inside fruit differs between cultivars, due to differences in diffusion and respiration properties, shape and size. As a result, optimal storage conditions differ between fruit cultivars (Ho et al., 2013). Because diffusion and respiration properties and fruit shape affect gas exchange in CA storage, variability of these parameters potentially introduces large uncertainty in respiration during storage. Process design should thus account for the effect of variability and predict confidence limits of optimal conditions rather than fixed values (Hertog et al., 2007; Nicolaï et al., 2011; Scheerlinck et al., 2001).

The observed variability of diffusion and respiration properties of fruit is large (Ho et al., 2011, 2010b). The shape of biological products is often complex, and rather difficult to acquire and describe (Goñi et al., 2008; Mebatsion et al., 2011). In addition, a large variability is found between species and cultivars. We have, however, been able to generate 3D computer models of pome fruit (Rogge et al., 2013). The resulting geometrical models have the same variability as the biological variability in the original biological products. While these 3D geometrical models are directly available as CAD models, numerical modelling of respiratory gas transport

phenomena inside the fruit taking into account 3D geometrical variation of biological products has not been achieved yet.

The objective of this contribution was to model the gas exchange in pear fruit taking the effects of biological variability into account. First, the variability distribution of relevant model parameters is determined, including shape, tissue structure and respiration rate. Then, stochastic simulations are used to evaluate the uncertainty of internal respiratory gas concentrations of the fruit and evaluate the consequences for susceptibility to storage disorders under optimal and sub-optimal conditions.

2. Material and methods

2.1 Materials

Pears (*Pyrus communis* 'Conference') were picked from the experimental orchard of the Research Station of Fruit Growing (Velm, Belgium). Fruit was harvested at two stages: in the optimal picking period (on 9th September, 2010) and in the late picking period (on 16th September, 2010). Fruits were cooled and stored according to commercial protocols for a period of 21 days at -1 °C followed by controlled atmosphere conditioning (2.5 kPa O_2, 0.7 kPa CO_2, -1 °C) up to the time of the experiment. Picking dates and cooling procedures were according to optimal commercial practices used for long-term storage of fruit.

2.2 3D shape generation

An enhanced version of the geometric model generator described in (Rogge et al., 2015) was used to create the required 3D geometric models of pear fruit. The model generator is able to accurately represent all shape features of the 3D outer contour of the pears. The model

generating algorithm that uses a 2D Fourier series expansion was developed based on surface contours extracted form X-ray Computed Tomography images of 66 'Conference' pears (Rogge et al., 2013). After statistical analysis of the obtained descriptors for all pears, new descriptors were generated, representing the studied distributions of descriptors. With the inverse of the shape description method, these new descriptors were transformed into smooth geometries, fit as CAD import for the simulations. The geometries were meshed with Comsol 3.5 (Comsol AB, Stockholm).

2.3 Diffusion-reaction model of gas exchange in pear fruit

The diffusion-reaction model of gas exchange that we developed earlier (Ho et al., 2010b, 2008) was used for stochastic simulations in this work. In this approach, tissues are considered to be homogeneous continuum materials. The effect of microstructural features (porosity and tortuosity) on gas transport is incorporated in the apparent value of the tissue properties.

Gas concentration gradients are the driving force for gas exchange. The continuum model thus contains diffusion and reaction terms:

$$\alpha_i \frac{\partial C_i}{\partial t} = \nabla \cdot D_i \nabla C_i + R_i \qquad (1)$$

with α_i the gas capacity of the component i (O_2 and CO_2) of the tissue (Ho et al., 2010b), D_i (m^2 s^{-1}) the apparent diffusion coefficient of the tissue, R_i (mol m^{-3} s^{-1}) the reaction term of the gas component i related to O_2 consumption or CO_2 production, ∇ (m^{-1}) the gradient operator, and t (s) the time. The time derivative in the left side of Equation (1) represents the concentration changes over time t (s) and becomes zero at equilibrium. Based on preliminary calculations we found that permeation could be neglected.

135 The gas capacity α_i is defined as:

136 $$\alpha_i = \varepsilon + (1-\varepsilon)\cdot R\cdot T\cdot H_i = \frac{C_{i,tissue}}{C_{i,g}} \quad (2)$$

137 where ε is the porosity of tissue, $C_{i,g}$ (mol m^{-3}) and $C_{i,tissue}$ (mol m^{-3}) are the concentrations of the
138 gas component *i* in the gas phase and the tissue, respectively. The concentration of the compound
139 in the liquid phase of fruit tissue normally follows Henry's law represented by the constant H_i
140 (mol m^{-3} kPa^{-1}). R (8.314 J mol^{-1} K^{-1}) is the universal gas constant and T (K) the temperature.
141 A non-competitive inhibition model (Hertog et al., 1998; Ho et al., 2010b; Lammertyn, 2001;
142 Peppelenbos and van't Leven, 1996) is commonly used to describe consumption of O_2 by
143 respiration:

144 $$R_{O_2} = -\frac{V_{m,O_2}.C_{O_2}}{\left(K_{m,O_2}+C_{O_2}\right).\left(1+\frac{C_{CO_2}}{K_{mn,CO_2}}\right)} \quad (3)$$

145 with V_{m,O_2} (mol m^{-3} s^{-1}) the maximum oxygen consumption rate, C_{O_2} (mol m^{-3}) the O_2
146 concentration, C_{CO_2} (mol m^{-3}) the CO_2 concentration, K_{m,O_2} (mol m^{-3}) the Michaelis-Menten
147 constant for O_2 consumption, K_{mn,CO_2} (mol m^{-3}) the Michaelis-Menten constant for non-
148 competitive CO_2 inhibition, and R_{O_2} (mol m^{-3} s^{-1}) the O_2 consumption rate of the sample.
149 The equation for production rate of CO_2 consists of an oxidative respiration part and a
150 fermentative part (Peppelenbos et al., 1996):

151 $$R_{CO_2} = -r_{q,ox}.R_{O_2} + \frac{V_{m,f,CO_2}}{\left(1+\frac{C_{O_2}}{K_{m,f,O_2}}\right)} \quad (4)$$

with V_{m,f,CO_2} (mol m^{-3} s^{-1}) the maximum fermentative CO_2 production rate, K_{m,f,O_2} (mol m^{-3}) the Michaelis-Menten constant of O_2 inhibition on fermentative CO_2 production, $r_{q,ox}$ the respiration quotient at high O_2 concentration, and R_{CO_2} (mol m^{-3} s^{-1}) the CO_2 production rate of the sample. At the fruit surface the following boundary condition is assumed:

$$-D_i \frac{\partial C_i}{\partial n} = h_i \left(C_i - C_{i,\infty} \right) \quad (5)$$

with n the outward normal to the surface; the index ∞ referring to the gas concentration of the ambient atmosphere; h_i the peel permeability for gas i (m s^{-1}), which represents the resistance of the peel. Values of model parameters are given in Table 1 with the respective source.

The continuum gas exchange model was numerically solved using the finite element method (Comsol 3.5, Comsol AB, Stockholm). Randomly generated 3D pear geometries described in Section 2.3 were employed to calculate the spatial profiles of internal gas concentrations of O_2 and CO_2 as a result of gas exchange, respiration and fermentation. A finite element mesh with local free mesh-element sizes was generated on the pear geometry. Eqs (1), (3)- (5) were discretised over this mesh and solved using Comsol.

2.4 Tissue structure and diffusivity

Diffusivity of tissue was calculated from a microscale model (Ho et al., 2011; Verboven et al., 2013). Briefly, the microscale diffusion model explicitly accounts for the transport of O_2 and CO_2 in the intercellular space, through the cell wall and plasmalemma into the cytoplasm, and incorporates the actual tissue microstructure as obtained from synchrotron radiation tomography images (Verboven et al., 2008). Six samples with a size of (0.84×0.84×1.43) mm^3 were used for the simulations. To determine the diffusivity of O_2 and CO_2 of a sample, (arbitrary)

concentration differences were applied over the microscale geometry, and the corresponding fluxes were computed by means of the microscale model (Ho et al., 2011; Verboven et al., 2013). From the fluxes and the length of the sample, apparent diffusivities were calculated. The computed O_2 and CO_2 diffusivities with six sample size of 0.84×0.84×1.43 mm^3 were equal to (2.01±2.98)×10^{-8} m^2s^{-1} and (2.62±2.97)×10^{-8} m^2s^{-1}, respectively. Variation of diffusivity was found among the samples. Increasing the sample size reduced the variation of the calculated apparent O_2 and CO_2 diffusivity.

2.5 Respiration kinetics

A non-competitive inhibition model was used to describe respiration kinetics of fruit tissue. The Michaelis-Menten constant K_m value for O_2 and CO_2 was considered as non-variable (Hertog et al., 1998) and taken from Ho et al. (2013) (See Table 1). The maximal respiration rate V_m (both the maximal O_2 consumption rate and the maximal fermentative CO_2 production rate) is a function of the initially available enzyme concentration depending on fruit maturity (Hertog et al., 1998). To determine V_{m,O_2} and V_{m,f,CO_2}, respiration rate measurements were carried out at two gas conditions of 21 kPa O_2, 0 kPa CO_2, 79 kPa N_2 and 0 kPa O_2, 0 kPa CO_2, 100 kPa N_2, respectively. Briefly, fruit were placed in 1.7 L glass jars (2 fruit per jar) and flushed with two defined gas mixtures for at least 24 hours. For each gas condition, five replications were carried out at -1 °C and four replications were carried out at 10 °C and 20 °C. The jars were closed after 24 hours. The initial gas composition and pressure in the headspace of jars were measured by means of a gas analyser (Checkmate II, PBI Dansensor, Denmark) and pressure sensor (DPI 142, GE Druck, Germany, accuracy ±0.01%). The gas analyser had an accuracy of ±0.1% and ±0.5% of the O_2 reading and CO_2 reading, respectively. The analyser was calibrated against calibrated

197 mixtures (Air products N.V., Belgium). The headspaces were analysed again after 24 h. The gas
198 percentages were converted to partial pressures by multiplying with the measured total pressure.
199 The gas partial pressure was converted to molar concentration according to the ideal gas law.
200 The O_2 consumption and CO_2 production rates were calculated from the difference in gas
201 concentration and the time lag between the two measurements and expressed in mole per volume
202 of sample (m^3 fresh volume of sample) and per unit time (s).

203 $$R_{i,fruit} = \frac{\Delta n_i \cdot V_{free}}{\Delta t \cdot V_{fruit}} \quad (6)$$

204 where $R_{i,fruit}$ (mol m^{-3} s^{-1}) is the O_2 consumption / CO_2 production rate of the component *i* (O_2
205 and CO_2); Δn_i (mol m^{-3}) and Δt (s) are the difference in gas concentration of the component *i* and
206 the time lag between the two measurements; V_{fruit} (m^3) and V_{air} (m^3) and are the volume of the
207 fruit and the free air volume of the jar, respectively.
208 In the validation experiments, intact fruits were placed in 1.7 L glass jars (2 fruit per jar) and
209 flushed with a gas mixture for 24 h. The composition of the latter was 21 kPa O_2 and 0 kPa CO_2
210 for the experiments at 10°C and 20°C. Four replicate measurements per gas concentration were
211 carried out. The O_2 and CO_2 gas partial pressures were monitored with a gas analyser and
212 pressure sensor with time interval of 1day during 10 and 15 days for the experiments at 20°C and
213 10°C, respectively. The respiration rate was calculated as mentioned before and compared to the
214 simulation result.
215
216 *2.6 Biological variation of model parameters*

Ho et al. (2013) found that V_{m,O_2}, V_{m,f,CO_2} and the gas diffusivities were the most important parameters beside the shape of fruit. For these parameters, a Monte Carlo analysis was performed to study the effects of biological variability. Hereto we generated 500 random parameter sets and for each set we solved the Eqs (1), (3)- (5). We considered only these parameters to be random and kept all other parameters fixed. For the random number generation of V_{m,O_2} and V_{m,f,CO_2} we assumed that these parameters were normally distributed with a standard deviation equal to that obtained from the parameter estimation procedure. Further, V_{m,O_2} and V_{m,f,CO_2} were assumed to be perfectly correlated (correlation coefficient equal to one) as they share a common pathway (glycolysis).

The tissue diffusivities of O_2 and CO_2 were also assumed to be perfectly correlated as they are all determined by the same tissue microstructure (Ho et al., 2011). In order to generate the apparent diffusivities, a Monte Carlo analysis was carried out. A series of 500 brick-like computational domains with a size of 2.52×2.52×2.86 mm^3 was constructed by assembling 18 (3×3×2) microscale zones. The O_2 and CO_2 diffusivity of each microscale zone was randomly selected from a set of diffusivity values computed based on 6 different cubical cortex tissue samples with a size of 0.84×0.84×1.43 mm^3. The corresponding flux over each of the computational domain was computed from an (arbitrary) concentration difference applied over the domain. The overall apparent diffusivity of each of the 500 computational domains was subsequently calculated from the corresponding flux. A normal distribution was fitted to these values.

To account for shape variability, 120 different pear geometries were produced by means of the shape generator.

239 *2.7 Simulations and analysis*

240 Monte Carlo simulations were performed for optimal CA storage conditions equal to 2.5 kPa O_2,
241 0.7 kPa CO_2 and -1 °C, for optimally picked and late picked pears. In addition, simulations were
242 performed for a range of different O_2 concentrations from 0.5 to 5.5 kPa.

243 For each storage condition, 500 random parameter combination sets of diffusivities and maximal
244 respiration rate were randomly chosen. For each set we solved the Eqs (1), (3)-(5) on a pear
245 geometry which was randomly selected from 120 different geometries. The Monte Carlo
246 simulations were carried out by integrating Comsol with Matlab (The Mathworks, Natick, MA)
247 using scripts programmed in the Matlab environment to perform the Monte Carlo simulations in
248 an automated way. In short, the 3D unstructured triangulated surface of a pear geometry was
249 imported into Comsol using CAD import module and the STL file format. A corresponding
250 volumetric geometry was reconstructed from the 3D unstructured triangulated surface and saved
251 as a geometry object with Comsol Multiphysic text file format (*.mphtxt). In each Monte Carlo
252 run for a particular storage condition, the 3D geometry object was randomly generated using the
253 geometrical model generator as described before and imported in Matlab with a script. A finite
254 element mesh was generated from the pear geometry using a default mesh generator function of
255 Comsol. Random parameter values for Eqs (1) and (3)-(5) where generated based on their
256 normal distribution function as described before. The model was then solved for steady state
257 conditions. Finally, the O_2 and CO_2 partial pressure profiles of Monte Carlo each run were
258 computed from the solution. For each storage condition, the run time for the Monte Carlo
259 simulation with 500 runs was about 4000 to 7000 s on a DUAL CPU Xeon X5650, 48 GB RAM.
260 From the simulations, the internal O_2 and CO_2 profiles of each fruit were obtained and the
261 minimal value of O_2 ($C_{O_2,\min}$) was determined. This value was compared to the critical O_2 level

below which fermentation dominates and disorder development was likely to occur. The critical O_2 level $C^*_{O_2}$ (kPa) was defined as the critical O_2 level of tissue where the ATP production rate due to the oxidative respiration is equal to maximal ATP production rate by fermentation. In other words, it is the O_2 concentration where the ATP production by oxidative respiration dominates the ATP production over that by fermentation (Ho et al., 2013).

$$C^*_{O_2} = \frac{f_f \cdot V_{m,f,CO_2} \cdot K_{m,O_2}}{f_o \cdot V_{m,O_2} \cdot r_{q,ox} - f_f \cdot V_{m,f,CO_2}} \quad (6)$$

where f_o (=6.33) and f_f (=1) are the stoichiometric coefficients of the ATP production due to the oxidative respiration and the fermentation, respectively (Ho et al., 2013). Since V_{m,O_2} and V_{m,f,CO_2} were assumed to be perfectly correlated (correlation coefficient equal to one) as they share a common pathway (glycolysis), $C^*_{O_2}$ in Eq. (6) was not sensitive to variations of these parameters either and could be considered as relatively stable.

3. Results

3.1 Random pear geometries

Some random shapes produced by the shape generator are shown in Fig. 1a. As a result of the chosen shape description method, the geometries contain some asymmetric, local shape features, that are also observed in real fruit. The histogram in Fig. 1b shows the spread of volumes of the generated geometric models.

3.2 Random O_2 and CO_2 diffusivities and maximal respiration rate

The gas diffusivity of fruit tissue is directly related to its micro-structure (Ho et al., 2011). Fig. 2a shows the simulated O_2 concentration distribution in the intercellular space of a typical parenchyma cortex sample using the microscale gas exchange model. The simulated gas concentrations in the small samples were significantly non uniform and depended to a large extent on the void distribution of the tissue sample. The distribution of the apparent diffusivity of O_2 and CO_2 is shown in Fig. 2b & 2c. The standard deviation of the tissue diffusivity of O_2 and CO_2 was, respectively, between 29% and 16% of their mean value. Because the microstructure of optimally and late picked fruit is not different (Verboven et al., 2008), the diffusivity did not depend on maturity.

V_{m,O_2} and V_{m,f,CO_2} are likely to be proportional to the initially available enzyme concentration (Hertog et al., 1998), and, hence, depend on fruit maturity. The measured V_{m,O_2} and V_{m,f,CO_2} of optimally picked pears were $(1.85\pm0.14)\times10^{-5}$ mol m^{-3} s^{-1} and $(1.78\pm0.17)\times10^{-5}$ mol m^{-3} s^{-1}, respectively. Histograms of randomly generated V_{m,O_2} and V_{m,f,CO_2} values are shown in Fig. 2d & 2e.

3.3 Validation of the macroscale model

The macroscale model was validated by comparing simulated values with measurements of overall fruit respiration rates at 10°C and 20°C (Fig. 3) of fruit that were not used for the model calibration. The model used the maximal respiration rate V_m (maximum O_2 consumption and maximum CO_2 production rates) obtained from measurements (see Table 1). Clearly, the model agreed well with the measured values and captured the characteristics of the respiratory response of intact fruit to O_2 availability. The O_2 concentration at which the O_2 consumption rate

304 decreased to half its maximal value was equal to 1.8 kPa and 4.8kPa at 10°C and 20°C,
305 respectively.

306 *3.4 Internal gas concentration profiles in CA condition*

307 Pear fruit is a biological material and is inherently affected by biological variation. Stochastic
308 simulation results of the O_2 and CO_2 distribution inside different fruit are shown in Fig. 4. Due to
309 the diffusion resistance of the cortex tissue, significant concentration gradients were established
310 inside the pear. A decrease of the O_2 partial pressure and an increase of the CO_2 partial pressure
311 towards the center of the fruit were observed. The concentration gradient in the cortex was steep
312 in pear fruit having a high maximal respiration rate, large volume and low diffusivity.
313 Histograms of the predicted $C_{O_2,\min}$ for two storage O_2 partial pressures computed with Monte
314 Carlo simulations at -1 °C are shown in Fig. 5. At a commercial storage O_2 partial pressure of 2.5
315 kPa, the variation of $C_{O_2,\min}$ of optimally picked pear was considerable, with internal
316 concentrations as low as 0.5 kPa (See Fig. 5b). In late picked pear, even lower values were found
317 (Fig. 5d). At storage oxygen partial pressures of 0.5 kPa, the internal oxygen concentration
318 dropped below 0.1 kPa (Fig. 5a & c).
319
320 *3.5 O_2 concentration in the fruit in response to the atmospheric O_2 level of low temperature CA*
321 *storage*

322 The model was applied to compute the smallest O_2 ($C_{O_2,\min}$) partial pressure inside the fruit for a
323 range of different storage O_2 partial pressures. For each storage condition, 500 Monte Carlo
324 simulations were carried out for variable diffusivities, maximal respiration rate V_m and fruit
325 shape. The calculated critical O_2 level $C_{O_2}^*$ was 3.81×10^{-2} kPa for optimally picked fruit. The

predicted $C_{O_2,\min}$ was then compared to $C^*_{O_2}$ to evaluate whether fermentation due to hypoxia would occur inside the fruit. The computed $C_{O_2,\min}$ is shown in Fig. 5e for optimally picked fruit as a function of the O_2 partial pressure of the storage atmosphere at -1 °C. At 2.5 kPa O_2, $C_{O_2,\min}$ was mostly larger than $C^*_{O_2}$ indicating sufficient energy supply for maintaining cell integrity. However, the risk of fermentation inside pear fruit increased at a reduced O_2 level of 0.5 kPa.

3.6 Effect of picking time on the risk of fermentation during CA storage

Pear fruit is more sensitive to storage disorders when it is harvested late (Lammertyn et al., 2000). In this study late picking was 7 days after the optimal picking time. The measured V_{m,O_2} and V_{m,f,CO_2} of the late picked pear at -1 °C were $(2.32\pm0.41)\times10^{-5}$ mol m^{-3} s^{-1} and $(1.90\pm0.49)\times10^{-5}$ mol m^{-3} s^{-1}, respectively. We assumed that picking date would not have an effect on fruit size because in a typical harvest large fruit are picked first and small fruit are left on the tree to further grow and mature and thus to be picked at a later stage.

The late picked pear thus had a higher maximal respiration rate than the pear picked at the optimal picking time, while the tissue microstructure and thus diffusivity was the same. The simulation results showed that the minimal O_2 concentration for the optimal picked pears was larger than that of late picked pears. At 2.5 kPa O_2, the predicted $C_{O_2,\min}$ of the optimally picked and the late picked pears was (1.42±0.22) kPa and (1.16±0.30) kPa, respectively (Fig. 5b & 5d). At a very low O_2 concentration of 0.5 kPa, the predicted $C_{O_2,\min}$ of the optimally and late picked pears was (0.048±0.023) kPa and (0.028±0.019) kPa, respectively (Fig. 5a & 5c). Hence, late picked pear are clearly more susceptible to fermentation during CA storage than optimally

picked pear. The predicted $C_{O_2,\min}$ for late pick pear as a function of the storage O_2 partial pressure at -1 °C is shown in Fig. 5f. The increasing respiration rate due to late picking shifts the predicted $C_{O_2,\min}$ curves towards the bottom left in the figure compared to Fig. 5e.

3.7 Incidence of fermentation and browning disorder

The critical O_2 level $C^*_{O_2}$ can be interpreted with respect to the parameters of the respiration and fermentation kinetics (Ho et al., 2013). We assumed that if the local O_2 level of pear fruit was lower than $C^*_{O_2}$, fermentation due to hypoxia would be likely to occur. The probability of fermentation inside pear fruit was thus calculated for a set of 500 stochastic simulations for each condition. The results are shown in Fig. 6. The occurrence of fermentation was high at 0.5 kPa O_2 (35.8% and 74% for optimally and late picked pears, respectively) but rapidly decreased when the ambient O_2 level increases.

To compare these results to previous experimental data, a logistic regression model proposed by Verlinden et al. (2002) was used to predict the incidence of browning disorder at different O_2 levels. The results are shown in Fig. 6b. At a commercial storage O_2 partial pressure of 2.5 kPa, the predicted incidence of storage disorder was indeed low. At a very low storage O_2 partial pressure of 0.5 kPa, the predicted incidence of browning disorder for the optimally and the late picked pears rapidly increased with storage periods from 4 to 36 weeks. Both models show that the probability of fermentation and browning disorder in pear fruit is high when the O_2 partial pressure was 0.5 kPa but rapidly reduced when the O_2 partial pressure increased to 2.5 kPa.

3.8 Effect of fruit size on the risk of fermentation during CA storage

Simulations were carried out for different fruit volumes in CA (2.5 kPa O_2, 0.7 kPa CO_2). Histograms of $C_{O_2,\min}$ for different fruit volumes with random diffusion and respiration parameters are shown in Fig. 7. Clearly, the risk of fermentation is high for large and late picked fruit when they are stored in CA, for which the distribution considerably shifts towards the left. The results show that increasing the fruit size reduced $C_{O_2,\min}$ and, hence, increased the risk of fermentation.

4. Discussion

Transport phenomena are important but complex processes in food process and preservation operations. Mathematical modeling serves to improve our understanding of the phenomena, and, more importantly, for designing and optimizing food processes (Datta, 2008; Feyissa et al., 2012; Ho et al., 2013; Perrot et al., 2011; Torrez Irigoyen et al., 2014) in a virtual way by simulation. As we demonstrated here for controlled atmosphere storage of pear fruit, such an approach must account for the complex and variable structure, shape, size and physiological properties of the food through stochastic simulation techniques (Hertog et al., 2007; Rogge et al., 2013; Scheerlinck et al., 2001; Serment-Moreno et al., 2015). In this way, risks can be better evaluated raising confidence in simulation approaches by the food industry.

The O_2 diffusivity in pear cortex tissue for different batches of pear has been shown to vary from 2.8×10^{-10} m^2 s^{-1} to 5.63×10^{-10} m^2 s^{-1} (Ho et al., 2009, 2006). Schotsmans *et al.*(2003) found a value of $(4.3\pm1.7)\times10^{-10}$ m^2 s^{-1} for the O_2 diffusivity of pear cortex tissue while the O_2 diffusivity of fleshy tissue reported by Lammertyn *et al.* (2001) was 1.71×10^{-9} m^2 s^{-1}. The CO_2 diffusivity of

391 pear cortex tissue has been found to range from 1.7×10^{-9} to 5.32×10^{-9} (Ho et al., 2009, 2006;
392 Schotsmans et al., 2003). The apparent diffusivities computed from the microscale model were
393 thus one order of magnitude larger than previously measured values. This is likely due to the fact
394 that most reported measurements of diffusion properties of pear cortex tissue involved disk
395 shaped tissue samples. Cutting of the sample will cause leaking of the cytoplasm into the
396 micropores by capillary action that is difficult to avoid. Because oxygen diffusion is much faster
397 in gas than in liquid, the tissue diffusivity may thus be underestimated considerably. We verified
398 this hypothesis by showing that, based on simulations with blocked pores, leaking of the cellular
399 liquid into the micropores decreased the effective tissue gas diffusivity considerably
400 (unpublished results). For more porous fruit such as apple, pore leakage does not occur to the
401 same extent and it has been shown that measurement agree with the model predictions (Ho et al.,
402 2011).
403 Fruit shape, maximal respiration rate and diffusivities are the most important parameters
404 affecting the O_2 and CO_2 profiles inside the fruit (Ho et al., 2013). For 'Conference' pear studied
405 here, the fruit volume varied up to 57% of its mean value. Similarly, the O_2 and CO_2 diffusivities
406 of tissue had standard deviations of 29% and 16% of their mean value, respectively. We found
407 that the maximal respiration rate was less variable than shape and diffusivity. The standard
408 deviation of maximal respiration rate ranged from 8% to 18% of its mean value. This variation
409 had, however, a large impact on the O_2 and CO_2 concentration profiles and occurrence of
410 fermentation inside fruit during storage. At low O_2 condition (<1 kPa), a high incidence of
411 fermentation was predicted and this may cause physiological disorders.
412 These results have implications for novel CA approaches such as dynamic CA (DCA). In DCA,
413 the oxygen concentration in the air-tight storage room is allowed to decrease (by fruit

414 respiration) well below 1 kPa until the bulk of fruit produces a response signal that indicates that
415 the fruit switches to fermentation, upon which the oxygen concentration is increased by the
416 control system. Several methods have been proposed to measure the fermentation threshold
417 signal (Delele et al., 2013; Gasser et al., 2008; Prange et al., 2011; Veltman et al., 2003b).
418 Evidently from the current analysis, storage at low oxygen is more critical and accurate control is
419 required. Because the DCA control signal holds for the complete fruit load in the room (several
420 hundreds of tons), it is important to mimimize the variability in storage. From the current results,
421 it can be advised that, for DCA, variation of fruit size should be minimized (e.g., by presorting)
422 and batches from different sources and picking dates should be avoided (as these increase the
423 variability of respiration rates).
424 The critical oxygen level $C^*_{O_2}$ can be interpreted with respect to the parameters of the respiration
425 and fermentation kinetics (Ho et al., 2013). The value of $C^*_{O_2}$ for pear at -1 °C in this study was
426 3.81×10^{-2} kPa, which is in the order of magnitude of values found for apple (5.64×10^{-2} to
427 6.71×10^{-2} kPa Ho et al., 2013). The obtained value (equivalent to 0.8 µM in liquid) is
428 approaching the range of the K_m of cytochrome *c* oxidase, the terminal oxidase in plant
429 respiration, which has been measured in artificial media (0.10 - 0.12 µM, Rawsthorne and Larue,
430 1986; 1 µM, Taiz and Zeiger, 1993; 0.14 µM, Millar et al., 1994). The onset of fruit ripening
431 resulted in an increase of the metabolic process and initiated senescence (Masia, 2003).
432 Respiration is the main reason for the decrease of the O_2 concentration in the fruit. It is affected
433 by the maturity stage of fruit (Bulens et al., 2012). Late picked fruit was shown to have a high
434 respiration rate (Franck et al., 2007; Streif et al., 2003). Our simulations predict that late picked
435 fruit may be susceptible to fermentation during CA storage because of their high maximal

436 respiration rate. The occurrence of browning disorder has been shown to be rather non-uniform
437 in a whole batch (Lammertyn et al., 2000; Verlinden et al., 2002): some fruit may have the
438 disorder and other not, and the extent of the defects varies among fruit. Modelling of browning
439 disorder has been studied by means of a black box logistic regression model (Lammertyn et al.,
440 2000; Verlinden et al., 2002). This model predicted a high incidence of browning disorder at an
441 O_2 level of 0.5 kPa but a low incidence at a commercial storage O_2 level of 2.5 kPa. We found
442 similar trends in the occurrence of fermentation inside the fruit using a physical modeling
443 approach.
444
445 **5. Conclusions**
446 Gas exchange in pear fruit was studied using a continuum model taking into account random
447 variation of diffusivities, maximal respiration rate and the 3D morphology of fruit. We created
448 different 3D geometries to account for biological variation of fruit shape using a geometric
449 model generation algorithm. The model predicted that the O_2 and CO_2 gas profiles inside the
450 fruit were highly impacted by the O_2 and CO_2 diffusivity, the maximal respiration rate and the
451 3D morphology of fruit. We have thus shown that the model can be effectively used to predict
452 gas exchange behavior and to analyse the incidence of fermentation at reduced O_2 levels during
453 controlled atmosphere storage. Our model predicted that the fermentation inside the fruit would
454 rapidly increase when the storage O_2 level was lower than 1 kPa. The model confirmed that
455 picking time, and fruit size are important criteria affecting the risk of fermentation during CA
456 storage.
457
458 **Acknowledgements**

The authors thank the Research Council of KU Leuven (OT 08/023 & 12/055), the Flanders Fund for Scientific Research (project G.0645.13), and the Institute for the Promotion of Innovation by Science and Technology in Flanders (project IWT-120033 'TomFood') for financial support. This research was carried out in the context of the European COST Action FA1106 ('QualiFruit'). 3D imaging was achieved with the support of the Hercules Foundation (AKUL001(HER/09/016)) and a beamtime grant of the ESRF, Grenoble, France (experiment number MA222).

References

Bosch, V., Cilla, A., García-Llatas, G., Gilabert, V., Boix, R., Alegría, A., 2013. Kinetics of ascorbic acid degradation in fruit-based infant foods during storage. Journal of Food Engineering 116, 298–303. doi:10.1016/j.jfoodeng.2012.12.003

Bulens, I., Van de Poel, B., Hertog, M.L.A.T.M., De Proft, M.P., Geeraerd, A.H., Nicolai, B.M., 2012. Influence of harvest time and 1-MCP application on postharvest ripening and ethylene biosynthesis of "Jonagold" apple. Postharvest Biology and Technology 72, 11–19. doi:10.1016/j.postharvbio.2012.05.002

Datta, A.K., 2008. Status of Physics-Based Models in the Design of Food Products, Processes, and Equipment. Comprehensive Reviews in Food Science and Food Safety 7, 121–129. doi:10.1111/j.1541-4337.2007.00030.x

Delele, M.A., Nicolaï, B., Verboven, P., Verlinden, B.E., 2013. Storage of respiratory produce. US Patent 20,130,013,099, 2013; EP Patent 2,547,213, 2013; WO Patent 2,011,113,915, 2011.

Feyissa, A.H., Gernaey, K. V., Adler-Nissen, J., 2012. Uncertainty and sensitivity analysis: Mathematical model of coupled heat and mass transfer for a contact baking process. Journal of Food Engineering 109, 281–290. doi:10.1016/j.jfoodeng.2011.09.012

Franck, C., Lammertyn, J., Ho, Q.T., Verboven, P., Verlinden, B., Nicolaï, B.M., 2007. Browning disorders in pear fruit. Postharvest Biology and Technology 43, 1–13.

Fukuda, S., Yasunaga, E., Nagle, M., Yuge, K., Sardsud, V., Spreer, W., Müller, J., 2014. Modelling the relationship between peel colour and the quality of fresh mango fruit using

488 Random Forests. Journal of Food Engineering 131, 7–17.
489 doi:10.1016/j.jfoodeng.2014.01.007

490 Gasser, F., Eppler, T., Naunheim, W., Gabioud, S., Hoehn, E., 2008. Control of the critical
491 oxygen level during dynamic CA storage of apples by monitoring respiration as well as
492 chlorophyll fluorescence. ISHS Acta Horticulturae 796, 69–76.

493 Goñi, S.M., Purlis, E., Salvadori, V.O., 2008. Geometry modelling of food materials from
494 magnetic resonance imaging. Journal of Food Engineering 88, 561–567.
495 doi:10.1016/j.jfoodeng.2008.03.020

496 Herremans, E., Verboven, P., Bongaers, E., Estrade, P., Verlinden, B.E., Wevers, M., Hertog,
497 M.L.A.T.M., Nicolai, B.M., 2013a. Characterisation of "Braeburn" browning disorder by
498 means of X-ray micro-CT. Postharvest Biology and Technology 75, 114–124.
499 doi:10.1016/j.postharvbio.2012.08.008

500 Herremans, E., Verboven, P., Defraeye, T., Rogge, S., Ho, Q.T., Hertog, M.L. a. T.M.,
501 Verlinden, B.E., Bongaers, E., Wevers, M., Nicolai, B.M., 2013b. X-ray CT for quantitative
502 food microstructure engineering: The apple case. Nuclear Instruments and Methods in
503 Physics Research Section B: Beam Interactions with Materials and Atoms.
504 doi:10.1016/j.nimb.2013.07.035

505 Hertog, M.L.A.T.M., Lammertyn, J., Scheerlinck, N., Nicolaï, B.M., 2007. The impact of
506 biological variation on postharvest behaviour: The case of dynamic temperature conditions.
507 Postharvest Biology and Technology 43, 183–192. doi:10.1016/j.postharvbio.2006.09.014

508 Hertog, M.L.A.T.M., Peppelenbos, H.W., Evelo, R.G., Tijskens, L.M.M., 1998. A dynamic and
509 generic model of gas exchange of respiring produce: the effects of oxygen, carbon dioxide
510 and temperature. Postharvest Biology and Technology 14, 335–349. doi:10.1016/S0925-
511 5214(98)00058-1

512 Ho, Q.T., Verboven, P., Mebatsion, H.K., Verlinden, B.E., Vandewalle, S., Nicolaï, B.M., 2009.
513 Microscale mechanisms of gas exchange in fruit tissue. The New phytologist 182, 163–74.
514 doi:10.1111/j.1469-8137.2008.02732.x

515 Ho, Q.T., Verboven, P., Verlinden, B.E., Herremans, E., Wevers, M., Carmeliet, J., Nicolaï,
516 B.M., 2011. A three-dimensional multiscale model for gas exchange in fruit. Plant
517 Physiology 155, 1158–68. doi:10.1104/pp.110.169391

518 Ho, Q.T., Verboven, P., Verlinden, B.E., Lammertyn, J., Vandewalle, S., Nicolaï, B.M., 2008. A
519 continuum model for metabolic gas exchange in pear fruit. PLoS Computational Biology 4,
520 e1000023. doi:10.1371/journal.pcbi.1000023

Ho, Q.T., Verboven, P., Verlinden, B.E., Nicolaï, B.M., 2010a. A model for gas transport in pear fruit at multiple scales. Journal of Experimental Botany 61, 2071–81. doi:10.1093/jxb/erq026

Ho, Q.T., Verboven, P., Verlinden, B.E., Schenk, A., Delele, M.A., Rolletschek, H., Vercammen, J., Nicolaï, B.M., 2010b. Genotype effects on internal gas gradients in apple fruit. Journal of Experimental Botany 61, 2745–55. doi:10.1093/jxb/erq108

Ho, Q.T., Verboven, P., Verlinden, B.E., Schenk, A., Nicolaï, B.M., 2013. Controlled atmosphere storage may lead to local ATP deficiency in apple. Postharvest Biology and Technology 78, 103–112. doi:10.1016/j.postharvbio.2012.12.014

Ho, Q.T., Verlinden, B.E., Verboven, P., Vandewalle, S., Nicolaï, B.M., 2006. A permeation-diffusion-reaction model of gas transport in cellular tissue of plant materials. Journal of Experimental Botany 57, 4215–24. doi:10.1093/jxb/erl198

Lammertyn, J., 2001. Comparative study of the O_2, CO_2 and temperature effect on respiration between "Conference" pear cell protoplasts in suspension and intact pears. Journal of Experimental Botany 52, 1769–1777. doi:10.1093/jexbot/52.362.1769

Lammertyn, J., Aerts, M., Verlinden, B.E., Schotsmans, W., Nicolaï, B.M., 2000. Logistic regression analysis of factors influencing core breakdown in "Conference" pears. Postharvest Biology and Technology 20, 25–37. doi:10.1016/S0925-5214(00)00114-9

Lammertyn, J., Scheerlinck, N., Jancsók, P., Verlinden, B.., Nicolaï, B.., 2003. A respiration–diffusion model for "Conference" pears I: model development and validation. Postharvest Biology and Technology 30, 29–42. doi:10.1016/S0925-5214(03)00061-9

Lammertyn, J., Scheerlinck, N., Verlinden, B.., Schotsmans, W., M. Nicolaï, B., 2001. Simultaneous determination of oxygen diffusivity and respiration in pear skin and tissue. Postharvest Biology and Technology 23, 93–104. doi:10.1016/S0925-5214(01)00113-2

Li, L., Guan, J., He, J., 2011. Effects of harvesting time on fruit quality and internal browning of "Wonhuwang" pear during cold storage. Frontiers of Agriculture in China 5, 247–250. doi:10.1007/s11703-011-1093-3

Mannapperuma, J.D., Singh, R.P., Montero, M.E., 1991. Simultaneous gas diffusion and chemical reaction in foods stored in modified atmospheres. Journal of Food Engineering 14, 167–183. doi:10.1016/0260-8774(91)90006-E

Masia, A., 2003. Physiological effects of oxidative stress in relation to ethylene in postharvest produce, in: Hodges D.M. (Ed.), Postharvest Oxidative Stress in Horticultural Crops. Food Products Press, New York, pp. 165–197.

Mebatsion, H.K., Boudon, F., Godin, C., Pradal, C., Génard, M., Goz-Bac, C., Bertin, N., 2011. A novel profile based model for virtual representation of quasi-symmetric plant organs. Computers and Electronics in Agriculture 75, 113–124. doi:10.1016/j.compag.2010.10.006

Millar, A.H., Bergersen, F.J., Day, D.A., 1994. Oxygen affinity of terminal oxidases in soybean mitochondria. Plant Physiology and Biochemistry 32, 847–852.

Nicolaï, B.M., Egea, J.A., Scheerlinck, N., Banga, J.R., Datta, A.K., 2011. Fuzzy finite element analysis of heat conduction problems with uncertain parameters. Journal of Food Engineering 103, 38–46. doi:10.1016/j.jfoodeng.2010.09.017

Pedreschi, R., Franck, C., Lammertyn, J., Erban, A., Kopka, J., Hertog, M., Verlinden, B., Nicolaï, B., 2009. Metabolic profiling of "Conference" pears under low oxygen stress. Postharvest Biology and Technology 51, 123–130. doi:10.1016/j.postharvbio.2008.05.019

Peppelenbos, H.W., Oosterhaven, J., 1998. A theoretical approach on the role of fermentation in harvested plant products. Acta Horticulturae 464, 381–386.

Peppelenbos, H.W., van't Leven, J., 1996. Evaluation of four types of inhibition for modelling the influence of carbon dioxide on oxygen consumption of fruits and vegetables. Postharvest Biology and Technology 7, 27–40. doi:10.1016/0925-5214(96)80995-1

Perrot, N., Trelea, I.C., Baudrit, C., Trystram, G., Bourgine, P., 2011. Modelling and analysis of complex food systems: State of the art and new trends. Trends in Food Science & Technology 22, 304–314. doi:10.1016/j.tifs.2011.03.008

Pinheiro, J., Alegria, C., Abreu, M., Gonçalves, E.M., Silva, C.L.M., 2013. Kinetics of changes in the physical quality parameters of fresh tomato fruits (Solanum lycopersicum, cv. "Zinac") during storage. Journal of Food Engineering 114, 338–345. doi:10.1016/j.jfoodeng.2012.08.024

Prange, R.K., DeLong, J.M., Wright, A.H., 2011. Storage of pears using dynamic controlled-atmosphere (DCA), a non-chemical method. Acta Horticulturae 909, 707–717.

Rawsthorne, S., Larue, T.A., 1986. Metabolism under Microaerobic Conditions of Mitochondria from Cowpea Nodules. Plant Physiology 81, 1097–1102. doi:10.1104/pp.81.4.1097

Rogge, S., Beyene, S.D., Herremans, E., Hertog, M.L., Defraeye, T., Verboven, P., Nicolai, B.M., 2013. A Geometrical Model Generator for Quasi-Axisymmetric Biological Products. Food and Bioprocess Technology 7, 1783–1792. doi:10.1007/s11947-013-1169-6

Rogge, S., Defraeye, T., Herremans, E., Verboven, P., Nicolaï, B.M., 2015. A 3D contour based geometrical model generator for complex-shaped horticultural products. Journal of Food Engineering 157, 24–32. doi:10.1016/j.jfoodeng.2015.02.006

587 Saquet, A.A., Streif, J., Bangerth, F., 2003. Energy metabolism and membrane lipid alterations in
588 relation to brown heart development in "Conference" pears during delayed controlled
589 atmosphere storage. Postharvest Biology and Technology 30, 123–132. doi:10.1016/S0925-
590 5214(03)00099-1

591 Scheerlinck, N., Verboven, P., Stigter, J.D., De Baerdemaeker, J., Van Impe, J.F., Nicolai, B.M.,
592 2001. A variance propagation algorithm for stochastic heat and mass transfer problems in
593 food processes. International Journal for Numerical Methods in Engineering 51, 961–983.
594 doi:10.1002/nme.202

595 Schotsmans, W., Verlinden, B.., Lammertyn, J., Nicolaï, B.., 2003. Simultaneous measurement
596 of oxygen and carbon dioxide diffusivity in pear fruit tissue. Postharvest Biology and
597 Technology 29, 155–166. doi:10.1016/S0925-5214(02)00251-X

598 Schotsmans, W., Verlinden, B.E., Lammertyn, J., Peirs, A., Jancsók, P.T., Scheerlinck, N.,
599 Nicolaï, B.M., 2002. Factors affecting skin resistance measurements in pipfruit. Postharvest
600 Biology and Technology 25, 169–179. doi:10.1016/S0925-5214(01)00170-3

601 Serment-Moreno, V., Deng, K., Wu, X., Su, Y.-C., Fuentes, C., Antonio Torres, J., Welti-
602 Chanes, J., 2015. Monte Carlo analysis of the product handling and high-pressure treatment
603 effects on the Vibrio vulnificus risk to raw oysters consumers. Journal of Food Engineering
604 144, 86–92. doi:10.1016/j.jfoodeng.2014.07.014

605 Streif, J., Saquet, A., Xuan, H., 2003. CA-related disorders of apples and pears. Acta
606 Horticulturae 600, 223–230.

607 Taiz, L., Zeiger, E., 1993. Plant physiology. The Benjamin/Cummings Publishing Company Inc ,
608 California.

609 Torrez Irigoyen, R.M., Goñi, S.M., Giner, S.A., 2014. Drying–toasting kinetics of presoaked
610 soybean. A mathematical model considering variable diffusivity, shrinkage and coupled
611 heat transfer. Journal of Food Engineering 142, 70–79. doi:10.1016/j.jfoodeng.2014.06.002

612 Veltman, R.., Lenthéric, I., Van der Plas, L.H.., Peppelenbos, H.., 2003a. Internal browning in
613 pear fruit (Pyrus communis L. cv Conference) may be a result of a limited availability of
614 energy and antioxidants. Postharvest Biology and Technology 28, 295–302.
615 doi:10.1016/S0925-5214(02)00198-9

616 Veltman, R.., Verschoor, J.., van Dugteren, J.H.R., 2003b. Dynamic control system (DCS) for
617 apples (Malus domestica Borkh. cv "Elstar"): optimal quality through storage based on
618 product response. Postharvest Biology and Technology 27, 79–86. doi:10.1016/S0925-
619 5214(02)00186-2

620 Veltman, R.H., Sanders, M.G., Persijn, S.T., Pemppelenbos, H.W., Oosterhaven, J., 1999.
621 Decreased ascorbic acid levels and brown core development in pears (*Pyrus communis* L.

622 cv. Conference). Physiologia Plantarum 107, 39–45. doi:10.1034/j.1399-
623 3054.1999.100106.x

624 Verboven, P., Herremans, E., Borisjuk, L., Helfen, L., Ho, Q.T., Tschiersch, H., Fuchs, J.,
625 Nicolaï, B.M., Rolletschek, H., 2013. Void space inside the developing seed of *Brassica*
626 *napus* and the modelling of its function. The New phytologist 199, 936–47.
627 doi:10.1111/nph.12342

628 Verboven, P., Kerckhofs, G., Mebatsion, H.K., Ho, Q.T., Temst, K., Wevers, M., Cloetens, P.,
629 Nicolaï, B.M., 2008. Three-dimensional gas exchange pathways in pome fruit characterized
630 by synchrotron x-ray computed tomography. Plant Physiology 147, 518–27.
631 doi:10.1104/pp.108.118935

632 Verboven, P., Pedersen, O., Herremans, E., Ho, Q.T., Nicolaï, B.M., Colmer, T.D., Teakle, N.,
633 2012. Root aeration via aerenchymatous phellem: three-dimensional micro-imaging and
634 radial O2 profiles in Melilotus siculus. The New Phytologist 193, 420–31.
635 doi:10.1111/j.1469-8137.2011.03934.x

636 Verlinden, B.E., de Jager, A., Lammertyn, J., Schotsmans, W., Nicolai, B.M., 2002. PH—
637 Postharvest Technology: Effect of harvest and delaying controlled atmosphere storage
638 conditions on core breakdown incidence in 'Conference' pears. Biosystems Engineering 83,
639 339–347. doi:10.1006/bioe.2002.0127

640 Zerbini, P.E., Rizzolo, A., 2002. Loss of ascorbic acid during storage of Conference pears in
641 relation to the appearance of brown heart. Journal of the Science of Food and Agriculture
642 82, 1007–1013.

643 Zhou, Y., Pan, X., Qu, H., Underhill, S.J.R., 2014. Low temperature alters plasma membrane
644 lipid composition and ATPase activity of pineapple fruit during blackheart development.
645 Journal of bioenergetics and biomembranes 46, 59–69. doi:10.1007/s10863-013-9538-4

646

647

Figures

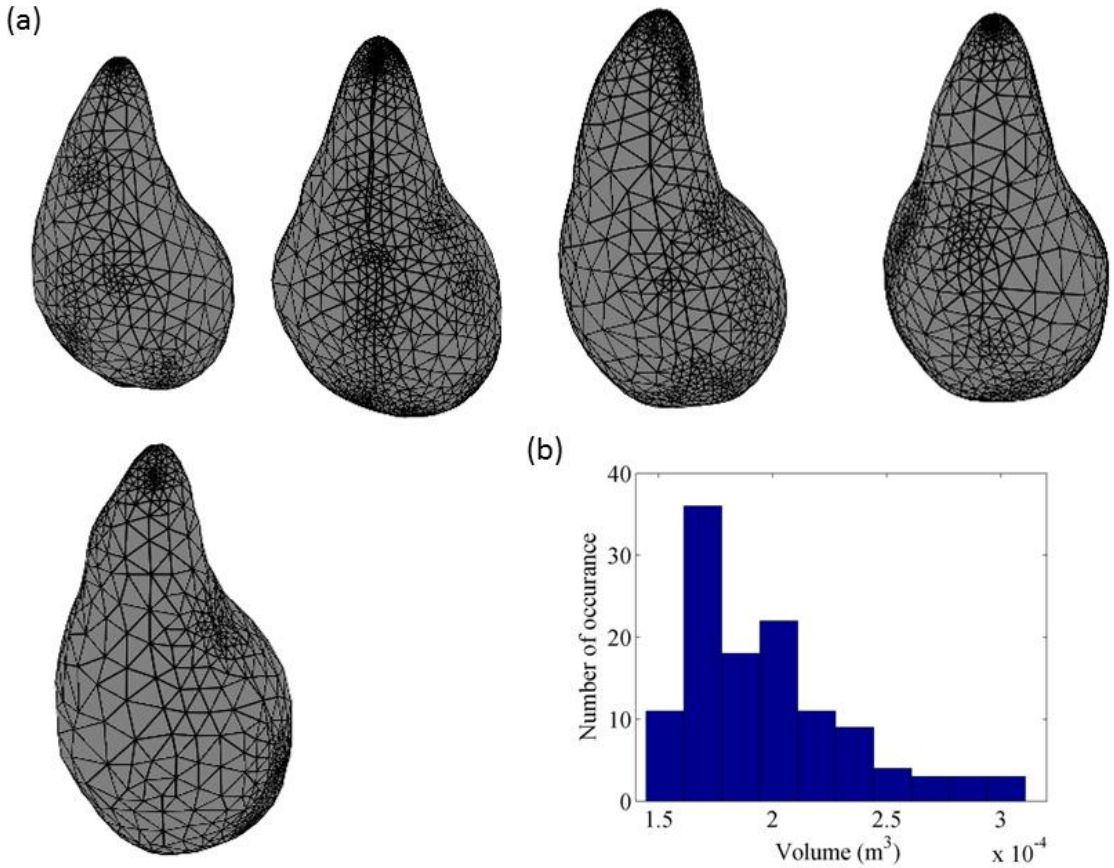

Fig. 1 Stochastic shape model of pear fruit: (a) Samples of generated geometrical models of Conference pear. (b) Distribution of volume of pear fruit obtained from 120 generated geometrical models.

655

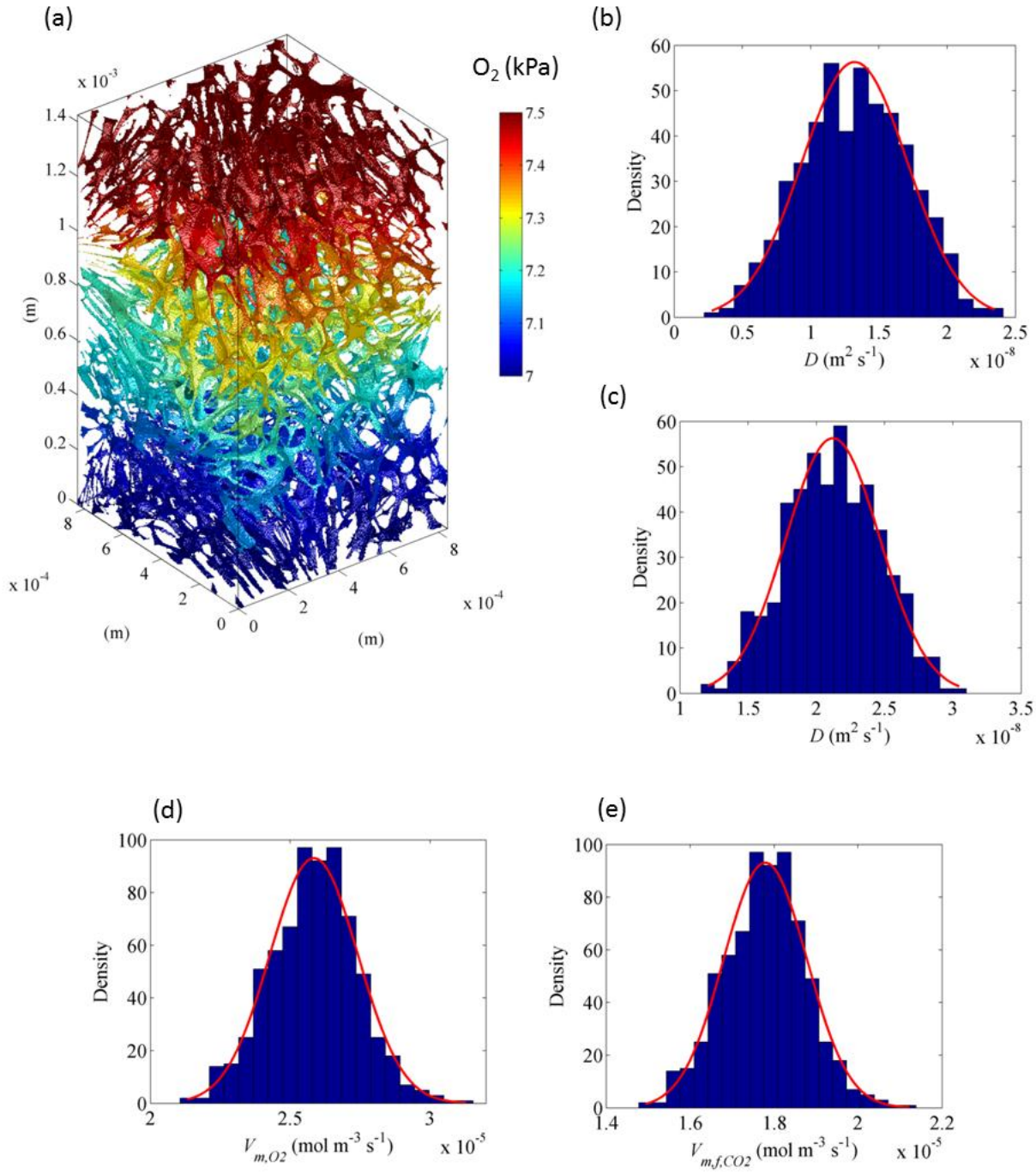

656

657 Fig. 2. Stochastic properties of pear fruit: (a) Simulated O_2 distribution in microstructure of

658 cortex tissue of pear fruit. The color represents the O_2 concentration in the pores (mol m^{-3}) for a

gradient imposed over the sample. The flux through the sample is then calculated from which the diffusivity is obtained. (b) and (c) Probability density distributions of the overall apparent diffusivity of O_2 and CO_2, respectively, based on 500 Monte Carlo simulations using the random microstructures. (d) and (e) Probability density distributions of the maximal O_2 consumption rate V_{m,O_2} and the maximal CO_2 production rate V_{m,f,CO_2} generated from measured data and standard errors.

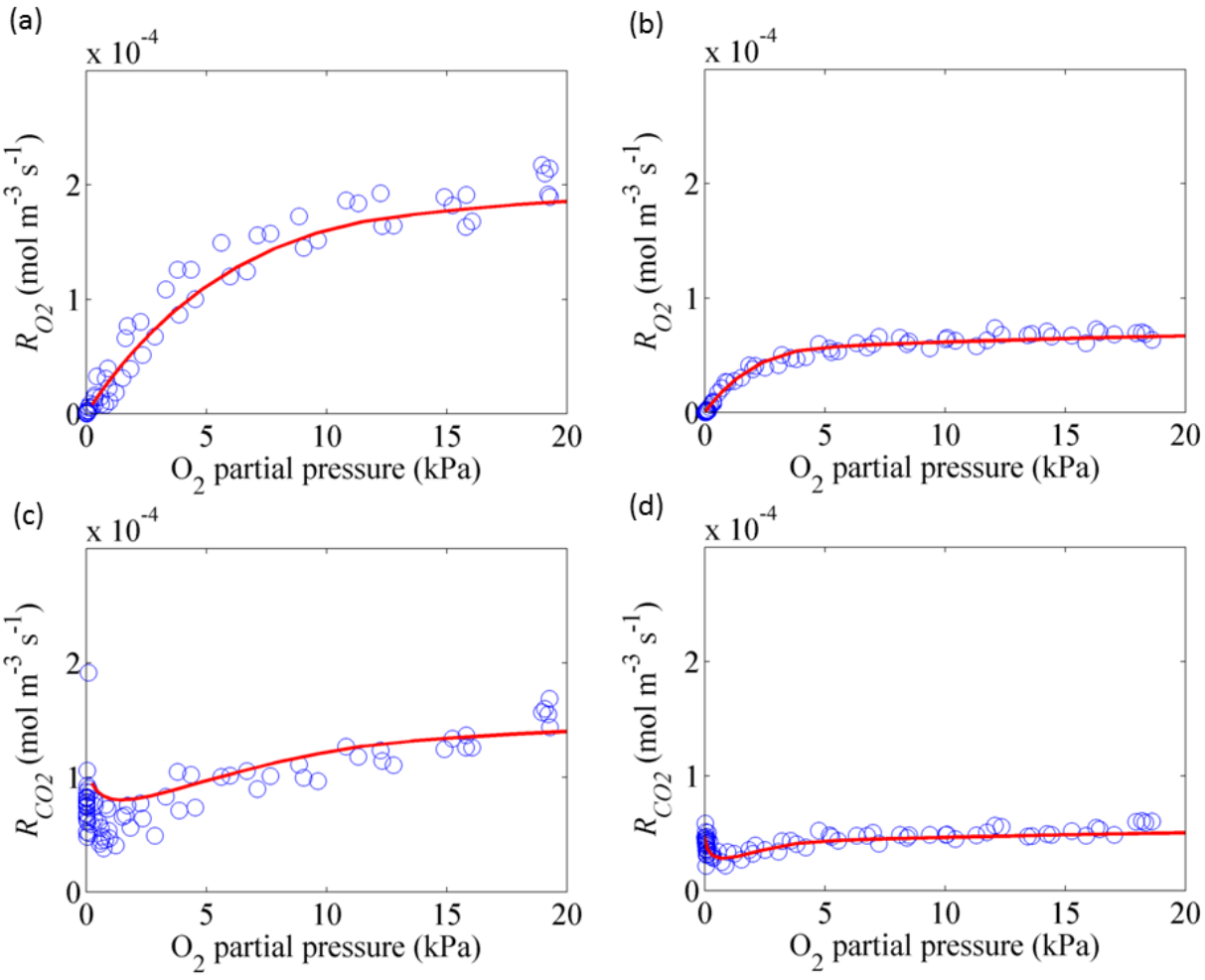

Fig. 3 Validation of the diffusion reaction model. O_2 consumption rate (R_{O2}) and CO_2 production rate (R_{CO2}) of intact pear fruit as a function of the O_2 concentration at 20°C (a, c) and 10°C (b, d). Symbols (o) indicate measurements and solid lines (—) correspond to simulations.

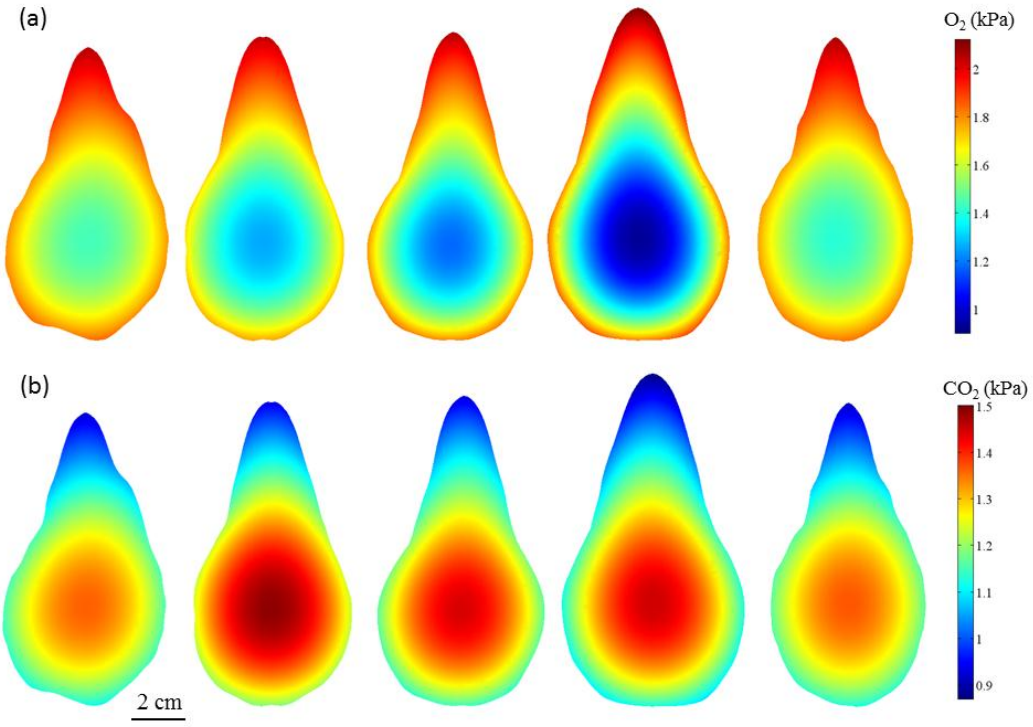

672

D_{O_2} (10^{-9} m^2 s^{-1})	16.9	15.2	10.4	6.89	16.5
D_{CO_2} (10^{-9} m^2 s^{-1})	23.7	22.4	19.1	16.0	25.0
V_{m,O_2} (10^{-5} mol $m^{-3}s^{-1}$)	1.90	2.16	1.92	1.61	1.85
V_{m,f,O_2} (10^{-5} mol $m^{-3}s^{-1}$)	1.83	2.14	1.85	1.49	1.77

673

674

675 Fig. 4. Examples of simulated O_2 and CO_2 partial pressure distributions in different intact pears
676 (vertical cross sections of the 3D pear model) at commercial CA conditions of 2.5 kPa O_2, 0.7
677 kPa CO_2 and -1 °C. The variation of shape, cortex diffusivities and respiration rate was taken
678 into account and described in Fig. 1 & 2. Used parameters are given below the figure. The color
679 indicates gas partial pressure (kPa).

680

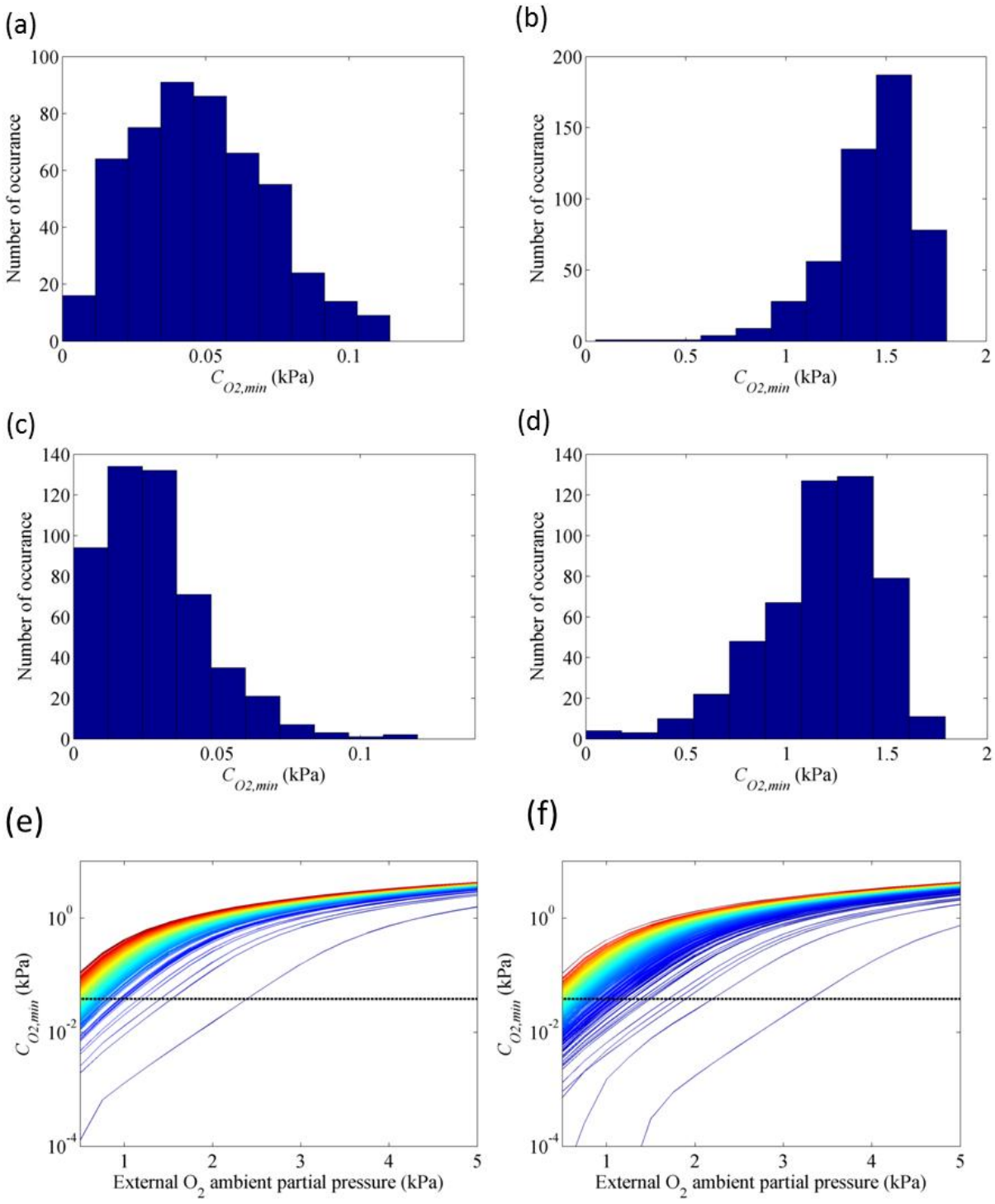
(a)
Number of occurance
$C_{O2,min}$ (kPa)
(b)
Number of occurance
$C_{O2,min}$ (kPa)
(c)
Number of occurance
$C_{O2,min}$ (kPa)
(d)
Number of occurance
$C_{O2,min}$ (kPa)
(e)
$C_{O2,min}$ (kPa)
External O_2 ambient partial pressure (kPa)
(f)
$C_{O2,min}$ (kPa)
External O_2 ambient partial pressure (kPa)

681

682 Fig. 5. Histogram of $C_{O_2,\min}$ at low external O_2 conditions computed with Monte Carlo
683 simulations at -1 °C for optimally picked pear (a & b) and late picked pear (c & d). (a) and (c)
684 are simulation results at 0.5 kPa O_2 while (b) and (d) are simulation results at 2.5 kPa O_2. (e) and
685 (f) Predicted $C_{O_2,\min}$ as a function of the ambient O_2 partial pressure at 0°C. Simulations take
686 variations in respiration capacity, diffusivity and shape of pear fruit into account. The horizontal
687 dashed (- -) line indicates the critical $C_{O_2}^*$. (e) and (f) represent simulations for the optimal
688 picked pear and late picked pear, respectively.
689

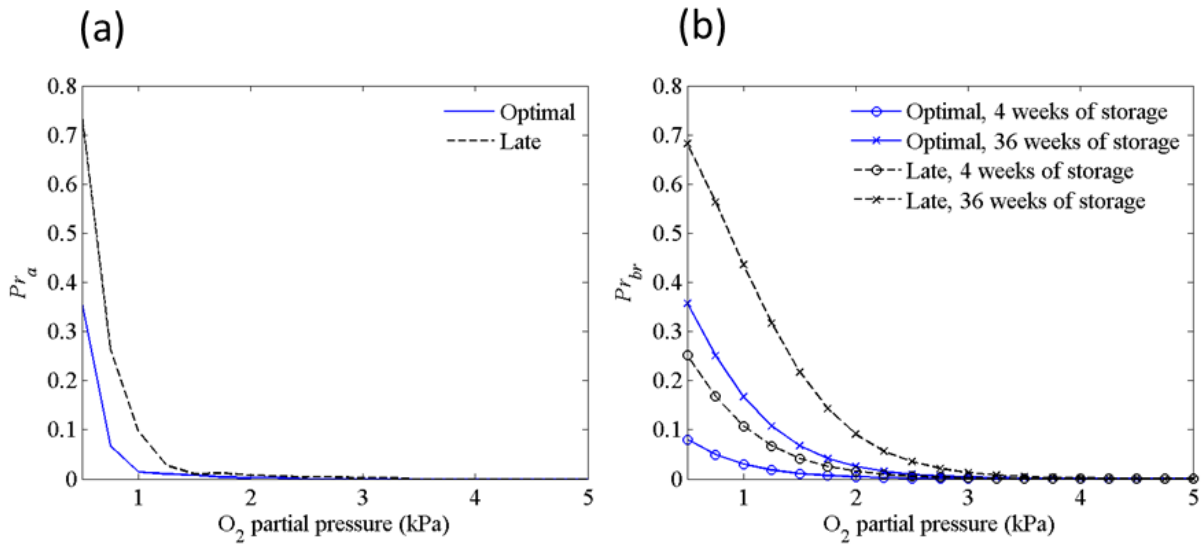

Fig. 6 Probability of fermentation (a) and browning disorder (b) of pear as a function of O_2 level. (a) Probability of fermentation (Pr_a) of optimally and late picked fruit predicted by the gas exchange model. (b) Probability of browning disorder of optimal and late picked fruit from 4 to 36 weeks predicted by the logistic regression model described by Verlinden et al. (2002).

699

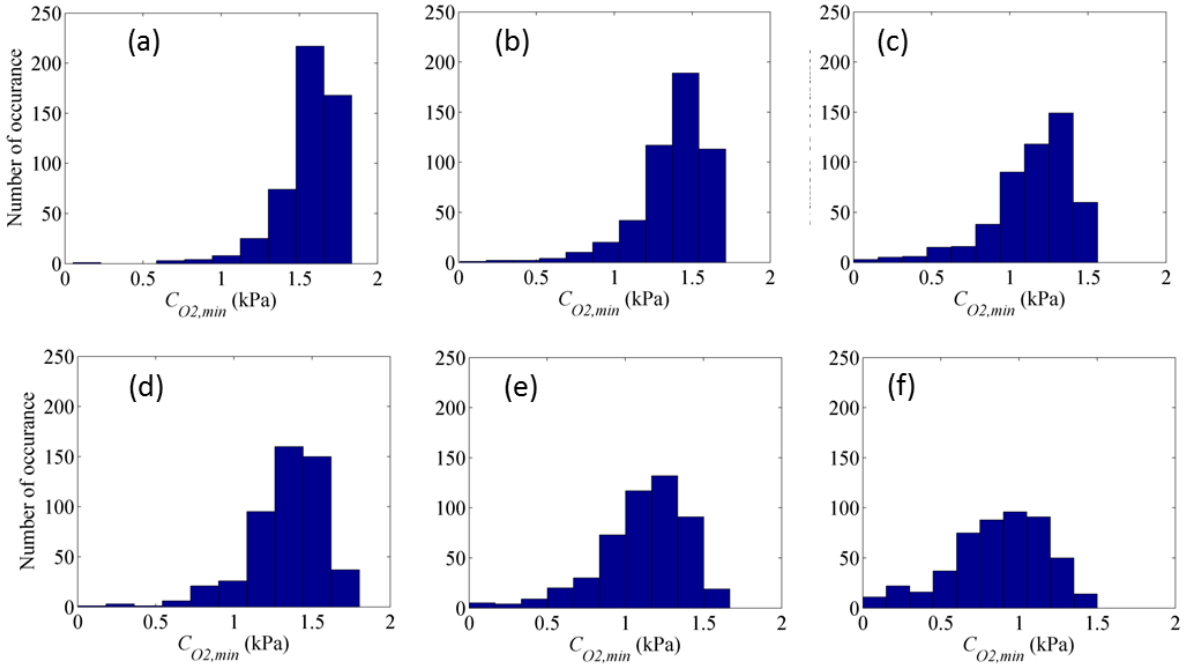

700

701 Fig. 7 Effect of fruit volume on the probability distribution of low oxygen concentration in pear.

702 Histograms of $C_{O_2,\min}$ are shown for increasing fruit volumes equal to 1.44×10^{-4} (a, d), 2.11×10^{-4}

703 (b, e) and 3.0×10^{-4} m^3 (c, f), respectively. Simulations were carried out at 2.5 kPa O_2, 0.7 kPa

704 CO_2 and -1 °C. (a), (b) and (c): optimally picked pear; (d), (e) and (f): late picked pear.

705

706

707 **Table 1 Parameters of macroscale gas transport model**

Physical parameters	O_2	CO_2
Diffusivity ($m^2\ s^{-1}$)		
Cortex tissue	$(2.01\pm2.98)\times10^{-8}$ (1)	$(2.62\pm2.97)\times10^{-8}$ (1)
($0.84\times0.84\times1.43\ mm^3$, n=6)		
Cortex tissue	$(1.32\pm0.39)\times10^{-8}$ (2)	$(2.12\pm0.34)\times10^{-8}$ (2)
($2.52\times2.52\times2.86\ mm^3$, n=500)		
Peel permeability ($m\ s^{-1}$)	8.77×10^{-7} (3)	7.48×10^{-7} (3)
Respiration parameters		
- K_{m,O_2} (kPa)		0.17 (4)
- K_{m,f,CO_2} (kPa)		2.4×10^{-2} (4)
-Maximal O_2 consumption rate V_{m,O_2} ($mol\ m^{-3}\ s^{-1}$)		
Optimally picked pear at 20°C		2.39×10^{-4}
Optimally picked pear at 10°C		6.8×10^{-5}
Optimally picked pear at 0°C		$(1.85\pm0.14)\times10^{-5}$
Late picked pear at 0°C		$(2.32\pm0.41)\times10^{-5}$
-Maximal CO_2 fermentative production rate V_{m,f,CO_2} ($mol\ m^{-3}\ s^{-1}$)		
Optimally picked pear at 20°C		1.15×10^{-4}
Optimally picked pear at 10°C		4.68×10^{-5}
Optimally picked pear at 0°C		

Late picked pear at 0°C	$(1.78\pm0.17)\times10^{-5}$
	$(1.90\pm0.49)\times10^{-5}$

708 (1) Computed from microscale model

709 (2)Apparent diffusivity of stochastic simulations for a larger sample containing random effective
710 diffusivities computed from simulated 3D microscale.

711 (3) Calculated from peel resistance of inert gas neon (Schotsmans et al., 2002) according to
712 Graham's law.

713 (4) Ho et al. (2013).